Multi-criteria assessment of a high-performance glulam through numerical simulation

Wilberth G Gomez-Ceballos, Mauricio Gamboa-Marrufo, Frédéric Grondin

Version of Record: https://www.sciencedirect.com/science/article/pii/S0141029622001675
Manuscript_81311f3e95730f3f3f58fd0790a90800

MULTI-CRITERIA ASSESSMENT OF A HIGH-PERFORMANCE GLULAM THROUGH NUMERICAL SIMULATION

Wilberth G. Gomez-Ceballos[a,b]
Mauricio Gamboa-Marrufo[a]
Frédéric Grondin[b] (frederic.grondin@ec-nantes.fr)
[a]Engineering Department, Universidad Autónoma de Yucatán, Avenida Industrias No Contaminantes por Periférico Norte, Yucatan, México, CP. 150 Cordemex
[b]Institut de Recherche en Génie Civil et Mécanique, UMR 6183, Centrale Nantes – Nantes Université – CNRS, 1 rue de la Noël, 44321 Nantes Cedex 3, France

Abstract

Timber-concrete structures have been developed as sustainable solutions to face current environmental challenges. This paper aims to present a numerical method for the analysis of the mechanical behaviour of glued laminated wood beams (Glulam) reinforced with ultra-high-performance fibre-reinforced concrete (UHPFRC). For this purpose, three series of a proposed Glulam-UHPFRC (HP-Glulam) beams with different slenderness ratio values, percentage, and position reinforcement under 4-point flexural tests were simulated by the finite element software Ansys®. The orthotropic linear elastic model was assigned to the Glulam, whilst to model the tensile plastic behaviour of UHPFRC the Cast Iron Model was adopted; this last model is based on grey cast iron. The numerical model results were validated with experimental tests from the literature. The Glulam beams increased their load capacity by up to 20 % with a cross-section composed of 11.36 % UHPFRC. The Series C, reinforced with a layer of UHPFRC at the top, demonstrated a greater increase in its flexural properties; therefore, the slender beams (span/depth = 13.16) were taken for a comparative analysis with concrete and steel beams. With the goal to propose a tool for building designers, estimation of costs and embodied energy generated during the production of materials were assessed too. Results show that

HP-Glulam beams is a potential substitute for frequently used concrete beams, with a production cost up to 56.16 % lower and up to 41.90 kgCO2e less embedded carbon.

Keywords: high-performance glulam, concrete-timber, failure, modelling, economic, CO_2 emission.

1. Introduction

The operational energy is reaching an optimisation limit, leaving the embodied energy in building materials as the next opportunity to reduce the environmental impacts of construction. On the other hand, carbon taxes are increasing every year as the carbon cap is lowered in favour of the Paris Agreement. This phenomenon and the underdeveloped design guidelines of natural and composite structures pose a challenge for the selection of green materials for new buildings.

Concrete is the most widely used building material in the world, responsible for 9 % of total greenhouse gas emissions [1]. This is indeed due to the use of cement, which is produced by grinding at very high temperatures in energy-intensive factories. Another important building material is steel, which is used as reinforcement for concrete structures or as structural elements. Steel accounted for an average of 3.5 to 4.5% of global CO_2 emissions in 2020 [2], [3]. Although the production of these building materials is being optimised to reduce their environmental impact, it will still take years to reach the performance of a natural material in terms of carbon emissions.

Bio-based materials such as timber and bamboo have been rediscovered as solutions to lightweight and decarbonize buildings. In a meta-analysis of 21 different

studies [4], it was concluded that an average of 2.1 tCO_2 could be saved for each tCO_2 in wood products used to substitute non-renewable building materials.

The transition to more sustainable materials allows for the use of composite structures that achieve the mechanical performance of current materials such as reinforced concrete. One proposed solution is to combine Ultra High-Performance Fibre Reinforced Concrete (UHPFRC) with Glue Laminated timber (Glulam). Studies have reported results of experimental measurements of elastic behaviour under a monotonic load and creep behaviour under a sustained load [5], [6], [7]. The importance of the bond between concrete and glulam and the increase of the stiffness of the reinforced members were shown. However, studies on the failure behaviour of this structure are not abundant. Statistical analyses on the main parameters of failure are insufficient and numerical modelling seems to be a suitable solution but is limited to elastic modelling [8]. The reason is that UHPFRC-Glulam (U-G) structure is a novel composite solution and failure tests to characterise all parameters for different designs are time-consuming and involve high CO_2 emissions. The design of U-G is complex due to the many possible concrete mixtures and different Glulam depths and adhesive types for bonding with concrete. Therefore, the investigation of the failure behaviour of these structures takes long time.

A new approach has emerged in civil engineering research that allows the optimization of experimental tests on selected trials. The method consists of developing a numerical model with consistent equations that accurately represent the behaviour of the structure, and boundary conditions that reproduce the real external conditions acting on the structure [9]. Simulations are performed for different sets of parameters to reproduce the maximum combination of material parameters with

boundary conditions representing all possible cases. The results permit to determine the relevant structural design for an experimental campaign. This approach reduces the number of experimental tests and saves a considerable amount of time. It provides engineers with a multi-criteria analysis for the optimised solution in terms of mechanical properties, economic gains, and environmental impact.

The formulation dependence of UHPFRC has complicated the standardisation of numerical models to describe its mechanical behaviour. In this sense, new models have been developed. However, some of them require complex tests to capture all parameters, such as the HJC model [10], and others are only capable of modelling a UHPFRC with strain-softening behaviour, such as the Ansys Concrete Model or the new Microplane model. However, the Cast Iron model has proven its efficiency in modelling beams in torsion and structural UHPFRC concrete sandwich panels [11], [12].

In this study, a numerical model was developed to simulate the ultimate behaviour of High-Performance Glulam (HP-Glulam) beams under flexural tests. The focus is on the analysis of the influence of the span-to-depth ratio and the amount and position of UHPFRC reinforcement. Indeed, it has been demonstrated on concrete and reinforced concrete [13] in three-point flexural tests that this ratio plays an important role on failure. The brittleness of concrete in the tensile area contributes to the kinetic of failure of the structure. The interest in UHPFRC is a better diffusion of internal stresses when the first micro-cracks appear into concrete, which could strength the flexure and shear behaviour of timber beams. Thus, the design of U-G beams needs to master the span-to-depth ratio to reduce an early failure risk. An economic calculation is also proposed to evaluate the industrial possibilities to manufacture the

proposed beams. Finally, an environmental assessment based on CO_2 emissions is proposed to complete a multi-criteria design decision tool for structural beams.

2. Materials and numerical method

2.1. Materials

In this investigation, glulam and UHPRRC are used to develop a High-Performance Glulam beam (HP-Glulam). Timber properties of an experimental composite beam study [5] were used. The timber body consisted of Fir 20F-E Douglas grade, with 36 mm thick laminates bonded with an epoxy paste (shear strength > 10 MPa). The selected Korean UHPC (K-UHPC) formulation and the experimental protocol were obtained from a test programme of UHPFRC I-beams under lateral torsional buckling [14]. This provided a UHPFRC with an elastic-linear behaviour in compression and in tension, where the elastic zone transitions to a plastic hardening zone (Fig. 1). Table 1 lists all the mechanical properties of the materials:

i) For UHPFRC: f_{cc} represents the compressive strength, ε_{cc} the ultimate compression strain, f_{ct} the elastic tension strength, ε_{ct} the limit elastic strain, f_{cp} the ultimate tension strength, ε_{cp} the ultimate tension strain.

ii) For MLE: f_{wc} represents the compressive strength, ε_{wc} the ultimate compression strain, f_{wt} the ultimate tension strength, ε_{wt} the ultimate tension strain.

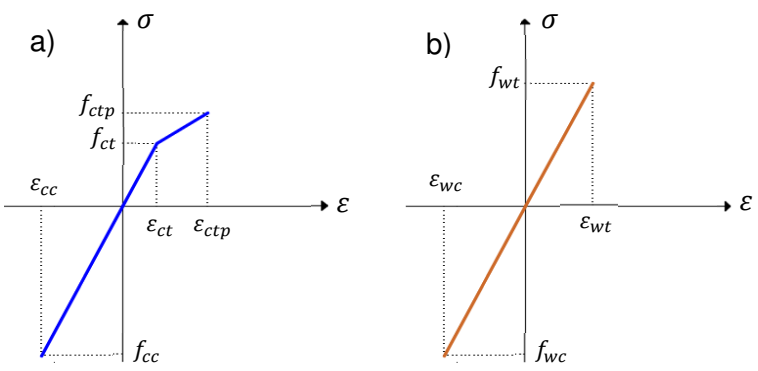

Fig. 1. Mechanical behaviour of the a) UHPFRC and b) timber (Adapted from [5])

Table 1. Mechanical properties of materials

UHPFRC						
f_{cc} (MPa)	ε_{cc} (‰)	f_{ct} (MPa)	ε_{ct} (‰)	f_{ctp} (MPa)	ε_{ctp} (‰)	E (MPa)
172	3.490[1)]	11.375	0.229	15.833	7.594	49 273
v		ρ (kg/m^3)				
0.2[2)]		2760				
MLE						
f_{wc} (MPa)	ε_{wc} (‰)	f_{wt} (MPa)	ε_{wt} (‰)	E_{xx} (MPa)	E_{yy} (MPa)	E_{zz} (MPa)
50	3.731[1)]	40	2.985[1)]	13 400	910	490
G_{xz} (MPa)	G_{xy} (MPa)	G_{yz} (MPa)	v_{xy}	v_{yz}	v_{zx}	ρ (kg/m^3)
300	710	730	0.4	0.4	0.2	500

1) Values calculated with Hooke's law. 2) Value obtained from [15].

2.2. Numerical method

2.2.1. Constitutive models

The reinforcement laminates are implemented in ANSYS using the Cast Iron model, which allows separating stress-strain responses in tension and compression. The tension behaviour is pressure-dependent and the Rankine maximum stress criterion is used:

$$f_t = \left(\sigma, \sigma_y^t\right) = \frac{2}{3} cos(\beta)\sigma_e + p - \sigma_y^t = 0 \quad (1)$$

where $p = \frac{1}{3} trace(\sigma)$ represents the hydrostatic pressure, $\sigma_e = \left(\frac{3}{2}\bar{\bar{\sigma}}:\bar{\bar{\sigma}}\right)^{\frac{1}{2}}$ the von Mises equivalent stress and $\beta = \frac{1}{3} cos^{-1}\left(\frac{3\sqrt{3}\,\bar{\bar{\sigma}}:\bar{\bar{\sigma}}}{\det(\bar{\bar{\sigma}})^{3/2}}\right)$, the Lode angle. In compression, the pressure-independent von Mises yield criterion is used:

$$f_c\left(\sigma, \sigma_y^c\right) = \sigma_e - \sigma_y^c = 0 \quad (2)$$

The evolution of the yield stresses follows the piecewise user-defined linear stress-strain curves for compression and tension. Detailed descriptions of the Cast Iron Model and its parameters can be found in Ansys User's Guide.

For the timber elements an orthotropic elastic behaviour law was assumed:

$$\begin{bmatrix}\sigma_{11}\\ \sigma_{22}\\ \sigma_{33}\\ \sigma_{12}\\ \sigma_{13}\\ \sigma_{23}\end{bmatrix} = \frac{1}{\Delta}\begin{pmatrix} \frac{1-\nu_{23}\nu_{32}}{E_2E_3} & \frac{\nu_{21}+\nu_{31}\nu_{23}}{E_2E_3} & \frac{\nu_{31}+\nu_{21}\nu_{32}}{E_2E_3} & & & \\ \frac{\nu_{12}+\nu_{13}\nu_{32}}{E_1E_3} & \frac{1-\nu_{31}\nu_{13}}{E_1E_3} & \frac{\nu_{32}+\nu_{31}\nu_{12}}{E_1E_3} & & & \\ \frac{\nu_{13}+\nu_{12}\nu_{23}}{E_1E_2} & \frac{\nu_{23}+\nu_{21}\nu_{13}}{E_1E_2} & \frac{1-\nu_{12}\nu_{21}}{E_1E_2} & & & \\ 0 & 0 & 0 & G_{12}\cdot\Delta & & \\ 0 & 0 & 0 & & G_{13}\cdot\Delta & \\ 0 & 0 & 0 & & & G_{23}\cdot\Delta \end{pmatrix}\begin{bmatrix}\epsilon_{11}\\ \epsilon_{22}\\ \epsilon_{33}\\ 2\epsilon_{12}\\ 2\epsilon_{13}\\ 2\epsilon_{23}\end{bmatrix} \quad (3)$$

With $\frac{\nu_{21}}{E_2}=\frac{\nu_{12}}{E_1}; \frac{\nu_{31}}{E_3}=\frac{\nu_{13}}{E_1}; \frac{\nu_{32}}{E_3}=\frac{\nu_{23}}{E_2}$ and $\frac{1}{\Delta}=\frac{E_1E_2E_3}{(1-\nu_{23}\nu_{32}-\nu_{31}\nu_{13}-\nu_{12}\nu_{21}-2\nu_{23}\nu_{31}\nu_{12})}$

The constants E, G y v are the Young's modulus, shear modulus and the Poisson's ratio according to the material planes.

The orthotropic model exhibited lower stiffness and caused greater deflections (~ 15 %) than the elastic isotropic model when used to replicate experimental results.

2.2.2. Simulation test set-up

Numerical simulations were first performed for each material to validate the mechanical models with the experimental results of the materials themselves. UHPFRC basic compression and tension tests were simulated to calibrate the Cast Iron model. The dimensions of the cylinder for compression (100 mm dia. X 200 mm) were taken from the Korean Concrete Institute (KCI) Recommendations [14]. The tension test has not been standardised, thus, a geometry (Fig. 2) capable of representing the plastic strain hardening behaviour was adopted from [16]. In addition, a prism (100 x 100 x 400 mm) according to the NF P18-470 [17] was used in a four-point flexural test to validate the numerical flexural behaviour of the K-UHPC

(Fig. 3). The modelled glulam beam used for validation replicated the geometry and loading configuration of the BLC-2m tested by Ferrier *et al*. [5].

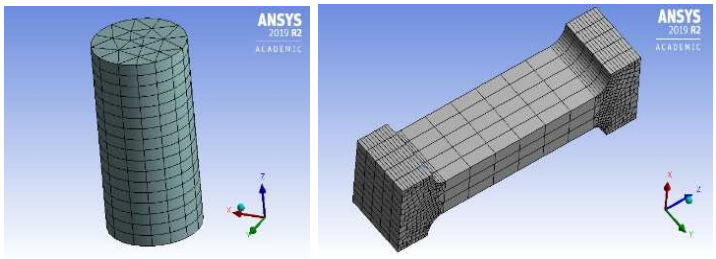

Fig. 2. Specimens for uniaxial compression (cylinder) and tension (dog bone) tests

For the composite beams, the UHPFRC flexural test set-up was chosen. The total dimensions of the composite cross-section were of 19.80 x 8 cm and remained the same for all the beams tested.

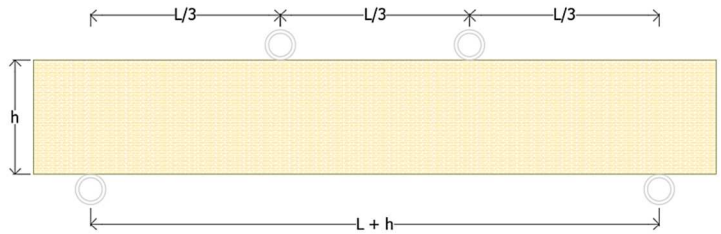

Fig. 3. Beam loading configuration

To investigate the effect of the span-to-heigh ratio (L/H) and the amount of UHPFRC reinforcement (ρ_{RC} = area of reinforcement / total area of cross-section) on the flexural behaviour, 15 HP-Glulam beams were modelled. To facilitate the casting process of the UHPFRC reinforcement in future studies, two 1.5 cm margins were left on each side and the height of a timber laminate was halved to maintain a commercial cross-section without modelling the epoxy paste. The spans and reinforcement configurations are given in Fig. 4 and Table 2. The beams are designated by the span-to-heigh ratio followed by a letter. Five unreinforced glulam

beams (BLC) were also simulated for flexural tests to compare the effectiveness of strengthened beams.

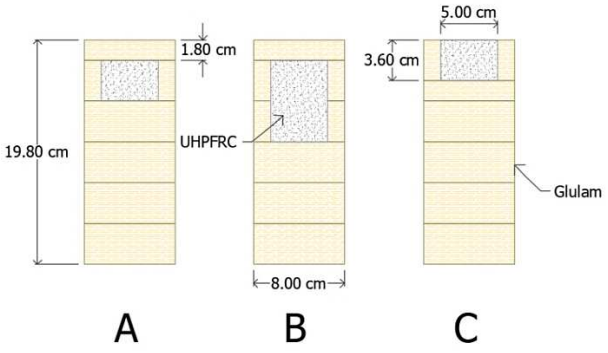

Fig. 1. Reinforcement of the cross-section: Series A and C: ρ_{RC} = 11.37 %; Series B: ρ_{RC} = 22.37 %

Table 2. Geometry of the composite beams

Model	BLCHP5-A/B/C	BLCHP7-A/B/C	BLCHP10-A/B/C	BLCHP13-A/B/C	BLCHP16-A/B/C
L (cm)	105	150	210	264	318
L/H	5.30	7.58	10.61	13.33	16.06

The supports were steel semicylinders to avoid excessive stress concentrations when loads were applied.

2.2.3. Element type and mesh

The SOLID186 mesh element was selected for all models. This higher order 3D 20-node element supports plasticity, stress stiffening and large strain capabilities. Moreover, its uniform reduced integration method prevents the volumetric mesh locking phenomenon that occurs in plasticity problems. The midside nodes, which were enabled for SOLID186 to increase the accuracy of the calculation, are not displayed by the software.

The U-G beam was discretised longitudinally with a mesh size between 2.5 – 3.8 cm, depending on the length of the beam, with a section mesh that allows continuity

between elements (Fig 5). Each timber laminate and UHPFRC reinforcement owned an independent mesh as they were created separately. Therefore, the compatibility between the nodes is enforced by the contact methods applied.

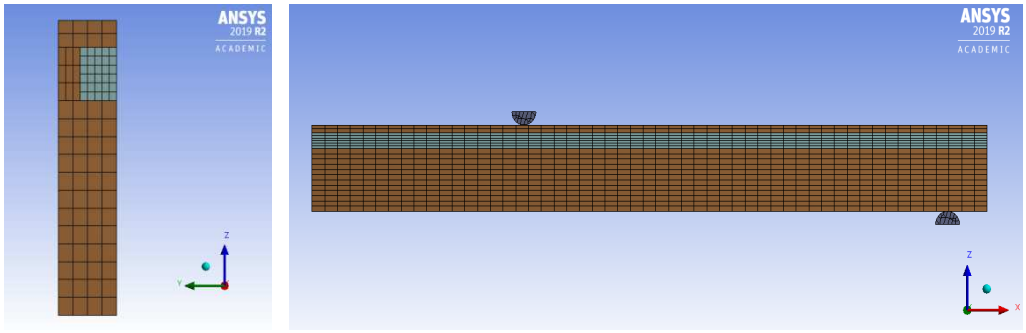

Fig. 5. HP-Glulam beam meshing

2.2.4. Contact assumption

The contact definition between rollers and beams was developed for the flexural tests. A perfect bond between timber and concrete layers is assumed, therefore it was assigned a *bonded-contact* behaviour to the interface of both materials. The result of this setting is a strain continuity between timber and concrete in all models (Fig. 6a). In fact, the strain profile experimentally confirmed that there was no slip at the interfaces between glulam and UHPFRC, as it followed a linear continuity between the materials [5]. All the beams tested in this study were instrumented with seven strain gauges at their mid-span. The strain profile of one of the composite beams is shown in Figure 6b. A linear strain between the concrete planks at the top and bottom of the main timber body can be seen; the same observation was made for all the specimens

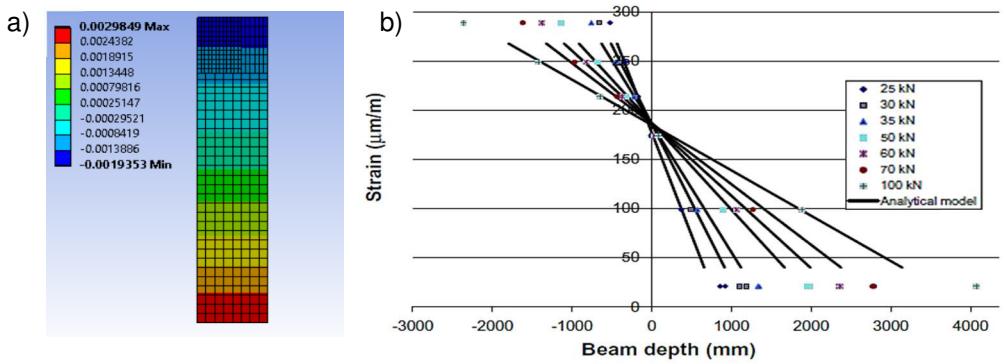

Fig. 6. Experimental results (a) (Adapted from [5]) and numerical results (b) of timber-concrete beams

Frictional-contact behaviour was used for the steel support and load rollers because the frictionless-contact behaviour underestimates the maximum load capacity. The asymmetric behaviour was chosen when defining the contact zones between the beam (target) and the rollers (contact). Since the friction coefficient depends on the tribology system [18], it was adjusted for both flexural tests to match the experimental conditions. Therefore, the coefficients of friction for concrete-steel and wood-steel contacts were 0.20 and 0.60, respectively.

2.2.5. Boundary conditions

Modelling is performed using displacement-controlled loading and the hypothesis of linear strain continuity between materials. Four boundary conditions (Fig. 7) were assumed in all numerical simulation tests: a) fixed support at the surface below the support roller; b) fixed displacement in the vertical (z) direction for the load roller with values ranging from 0.01 for shorter beams to 0.05 m for the larger ones; c) frictionless support at the outer surface of the beam normal to this plane; and d) double symmetry in the horizontal (x and y) direction to model only one quarter of the beam.

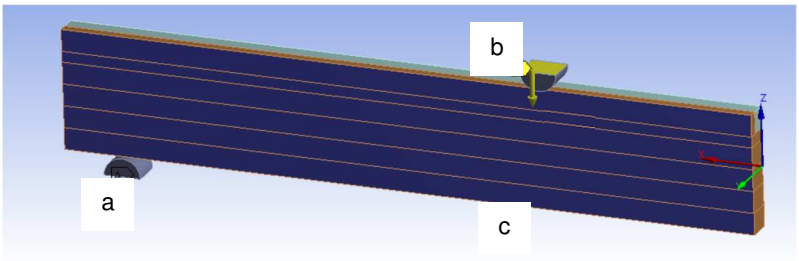

Fig. 7. Boundary conditions

2.3. Failure criteria

Materials such as timber and UHPFRC exhibit great variation in their properties due to their intrinsic nature. In general, the failure criteria most used in numerical simulations are based on uniaxial stress or deformation states, distortion energy or shear forces. Although, these failure criteria predict the limits of structures subjected to multiaxial stress states, they are not practical for the design of simpler structures, such as beams. Therefore, other methods, such as cross-section analysis, have been developed and included in the design codes (e.g. Eurocodes, ACI).

2.3.1. Flexural failure

In the sectional analysis, the compatibility and linearity of the deformations facilitate the determination of the rupture of a material, because the deformations are delineated, unlike the stresses, which may be unevenly distributed in a composite cross-section (Fig. 8). Thus, if the plane of deformation of a section passes through one of the limits of deformation of one of the materials, the beam would have failed. A pure flexural section is only subjected to tension and compression, which is true for the middle region in a four-point flexural test.

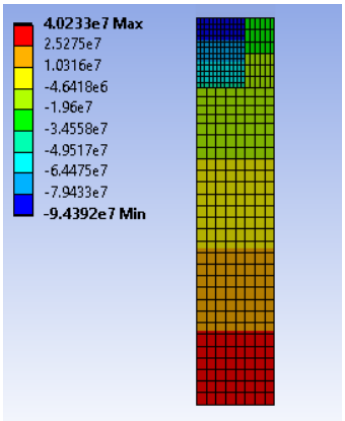

Fig. 8: Normal stress (Pa) distribution in the cross-section of a HP-Glulam

Therefore, the flexural failure criterion is defined by the maximum normal strain of the materials. Consequently, the following constraints were established by the compatibility of the deformations:

- in compression, the maximum normal deformation corresponds to the lowest deformation between UHPFRC and glulam.
- in tension, the maximum normal deformation corresponds to the maximum deformation of the wood;
- in the case of the flexural tests of each separated material, their respective maximum deformations were taken.

The three-dimensional aspect of the numerical simulation, allowing the orthotropic behaviour of the glulam and the tensile plasticity of the UHPFRC to be considered, required the use of planes in Ansys® software for the application of the failure criteria.

2.3.2. Shear failure

The span-to-height ratio of a beam influences its type of failure. Slender beams subjected to vertical loads develop a flexural failure, while short beams experience an

abrupt shear failure. The shear strength of UHPFRC calculated using the AFGC Recommendations [15] and the NF P-710 [19] was 16.50 MPa. Thus, based on the mechanical properties of the materials and the geometry of the composite beam, shear failure in U-G beam is controlled by the shear strength of the timber.

Verification of the shear strength of timber is assessed in the Eurocode 5 [20] with equation 4:

$$\tau_d \leq f_{wv,d} \quad (4)$$

The shear strength of timber beams presents a size effect. For this study, the shear strength was retained for the 4 x 8 and 4 x 12 inch sections, which correspond to 5.99 ± 0.79 and 5.02 ± 0.89 MPa [21], respectively. The value adopted to determine the failure of a beam was the minimum value within the specified range.

In the numerical simulation using Ansys® software, the application of the shear strength criterion was done by planes located in the central part between the supports and the load rollers. In this way, the maximum shear force at each load step was determined and compared with the values given by equation 4.

2.4. Completing the global performance assessment

2.4.1. Mechanical behaviour

Series C beams showed the greatest increases in load capacity and stiffness with a smaller volume of reinforcement. Therefore, beams with span-to-heigh ratio of 13 and 16 were retained for comparison. The revised parameters were the load capacity, the maximum moment of the cross-section and the deflection. The analysis was performed according to the Eurocodes [20], [22], [23], but without safety factors to evaluate the mechanical behaviour of each material.

For the steel beams, IPE 200 grade S235 was selected because its dimensions are very similar to those of the studied beams. The reinforced concrete beam has a

cross-section of 20 x 8 cm with a compressive strength of 25 MPa and the rebar class was B500B with a yield strength of f_{yk} = 500 MPa and a Young's modulus of E = 200 000 MPa; moreover, the use of longitudinal reinforcement was limited to tension only.

2.4.2. Production costs

The selection of materials and geometries of structural elements depends mainly on the manufacturing cost and the simplicity of the construction process. Therefore, the economic aspect of new structures should be included in the performance evaluation. The cradle-to-gate production cost analysis of the steel, reinforced concrete, timber, and composite beams comprised natural structural elements without flame retardants, fungicides, or moisture treatments. Given the versatility of the construction companies in installing structural elements, these costs were not included; instead, the labour required to fabricate the elements was considered. Prices for steel, reinforced concrete and timber beam were obtained from suppliers in France. UHPFRC production costs, on the other hand, vary as they are formulated on request depending on the mechanical, architectural and durability requirements of each project. Therefore, the average cost for Europe approximated by [24] in his analysis of 70 UHPFRC mixtures was used, plus 30 % of the labour cost required to produce the BLCHP beam.

2.4.3. Environmental evaluation

The indicator of embodied energy ($kgCO_2e$) was used to estimate the environmental impact of the beams. In this regard, the Environmental Product Declarations (FDES) governed by the French standard NF EN 15804+A1: "Sustainability of construction

works" and its national complement NF EN 15804/CN were employed. For this study, only the data of the production stage was taken, given by the standard. The production method is not studied while it could influence the final value of CO_2. The embodied energy of steel was calculated by [25]. In the case of timber, an FDES [26] was used for a GL24 Douglas beam, which is similar to the Canadian species used in the mechanical analysis. For the reinforced concrete beam, an adaptation of the FDES [27] of a described column was conducted, considering an equivalence to the volume and cross-section of the analysed beams.

The strong dependence on the formulation of the UHPFRC complicates the standardisation of the embodied energy consumed in its production. Then, the proportions of the K-UHPC from [28] and the detailed analysis of the constituents of a UHPFRC from [29] were combined to obtain an estimate of 0.4 $kgCO_2e/kg$. Table 3 summarises the embodied energy for each material used in the analysis.

Table 3. Embodied energy of materials

Material	$kgCO_2e/kg$
Reinforced concrete	0.12
Steel S235	1.40
GL24 Douglas timber	-1.48
K-UHPC	0.4

3. Results and discussions

3.1. Validation of the mechanical models

3.1.1. Analysis of the mechanical behaviour of UHPFRC

The use of the Cast Iron model to simulate the behaviour of UHPFRC was validated with experimental tests [14]. In compression, the difference between experimentally developed model and the finite element software Ansys® model was 0.54 % for maximum load, corresponding to a maximum deformation of 0.0035. The average

difference between the maximum load of each experimental test and the software Ansys® model was 8.62 %.

The simulation of the simple tension test served to validate the tensile behaviour of the UHPFRC and delimit its plastic zone, avoiding convergence problems. The average of the values obtained from 3 tests using the final tension model of [14] was compared with the results of the Cast Iron model. The numerical simulation showed that the Cast Iron can reproduce the hardening plastic behaviour of the UHPFRC in tension (Fig. 9). The differences between the experimental and numerical model for the maximum elastic and plastic deformations were 0.48 and 0.02 %, respectively.

The maximum compressive stress at the top of the UHPFRC beam cross-section was close to 100 MPa, while the calculated flexural strength was 44.20 MPa. The value of flexural strength is normalised with the formula of a homogeneous isotropic elastic beam, which explains the difference between the actual stresses and deformations of the cross-section. This flexural strength corresponds to a deviation of 1.69 % from the experimental tests.

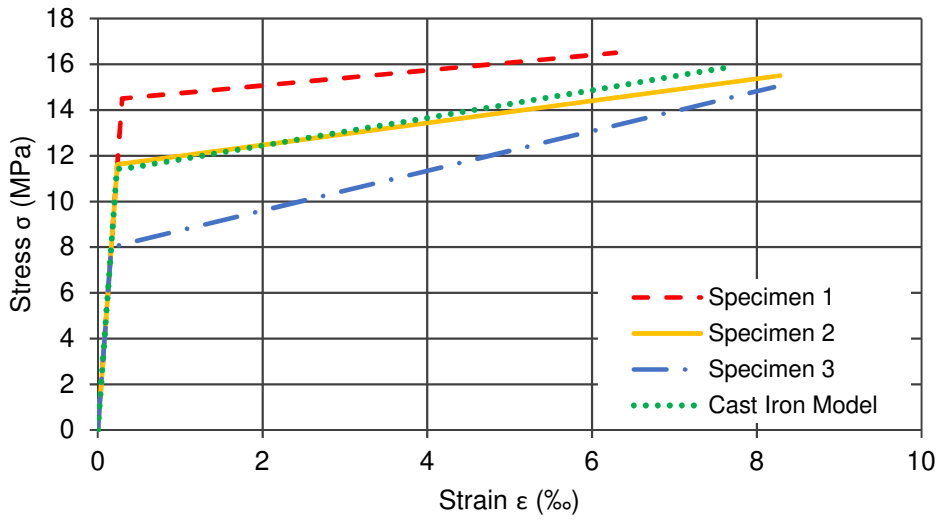

Fig. 9. Tensile stress-strain curve

3.1.2. Analysis of the behaviour of Glulam

The comparison of numerical and experimental results for Glulam beams is shown in Fig. 10, where a maximum moment for the simulated beam of 51.05 kNm is observed. The orthotropic elastic model showed a behaviour very close to the experimental and analytical results calculated by [5], with a difference for the peak load of 4 % between the numerical and experimental values (Table 4).

Table 4. Validation of flexural tests for Glulam

Maximal analytical load for shear failure (kN)	Maximal numerical load for shear failure (kN)[1)]	Maximal analytical load for flexural failure (kN)	Maximal numerical load for flexural failure (kN)[1)]	Maximal experimental load (kN)	V_{exp}/V_{teo}	V_{exp}/V_{num}
138.00	145.86	164.00	164.23	140.00	1.020	0.960

V_{exp}, V_{teo}, V_{num} represent maximal experimental, analytical and numerical loads. 1) These numerical results are compared to the values of [5].

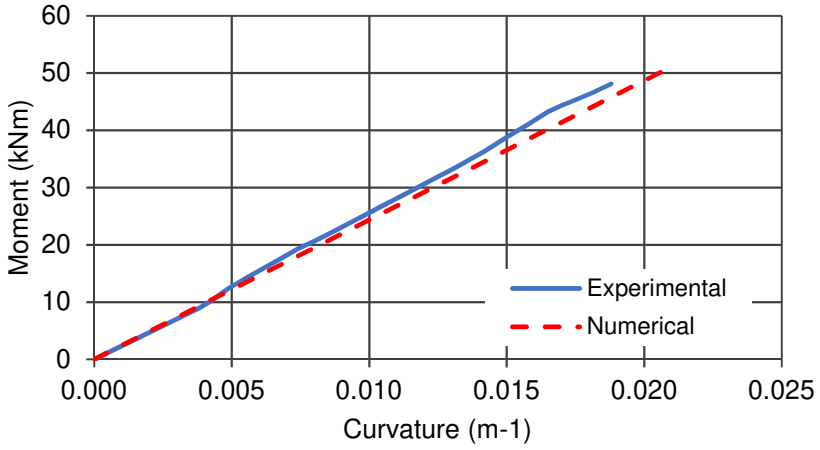

Fig. 10. Comparison of experimental and numerical moment-curvature relationships

3.2. HP-Glulam beam mechanical behaviour

3.2.1. Flexural behaviour

The relationship between load and deflection (Fig. 11) showed linear behaviour for all beams, even for Series B (reinforced with two concrete laminates), which developed

a plastic tension zone at the bottom of the UHPFRC cross-section. For the three series, the flexural stress led to a brittle failure in the extreme tension layer of the timber of the beams from L/H = 7.

A progressive development in the load capacity of Series A and C compared to the BLC beams can be observed. The largest increases were 11.59 and 20.10 % for beams with L/H = 16. For Series B, the load capacity increased up to beam BLCHP10-B, after which it started to decrease. This indicates that the amount of reinforcement limits the increase of the load capacity. The location of the reinforcement also proved to influence the load capacity. For instance, the BLCHP16-C resisted almost 10 % more than its equivalent type A. Thus, as the slenderness of the beams increases, the increase in the load capacity of the Series C outweighs the others.

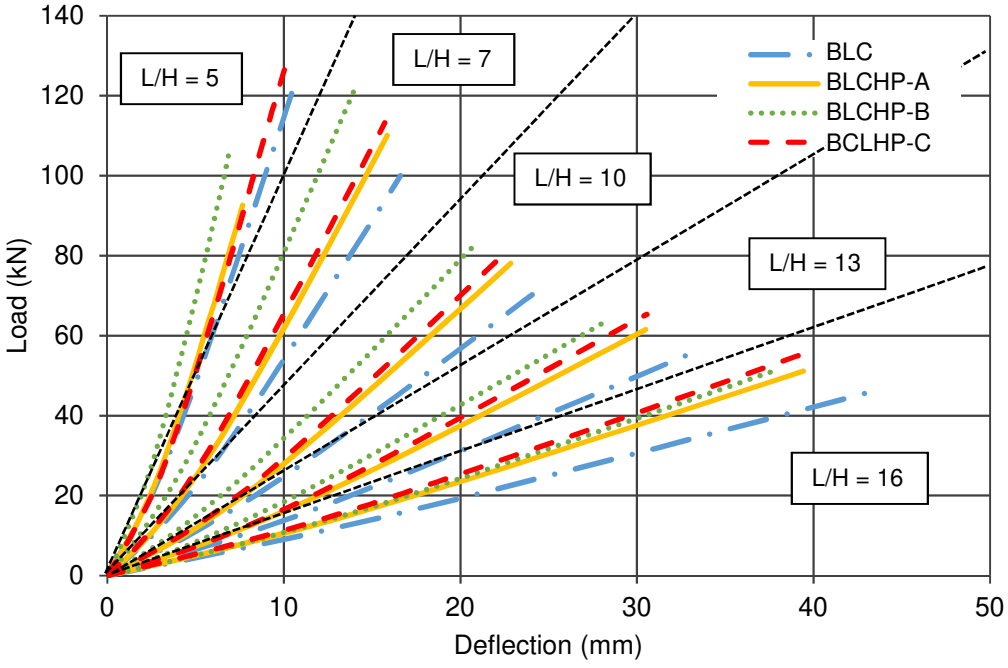

Fig. 11. Load-deflection of beams

Vertical displacements at the centre of the beams were reduced by using UHPFRC, being the Series B beams that had the lowest deflections due to the larger volume of reinforcement, with a deflection reduction of 27.78 % for BLCHP5-A. For Series C, the thinner the beam became, the greater the reduction in vertical displacement from a span-to-ratio of L/H = 10, with a maximum reduction11.14 % for BLCHP16-C.

During the simulations, the variation of the cross-section was given in the amount and the position of reinforcement, so the maximum flexural moment remained approximately constant for Series A, B, C and BLC. Series C (ρ = 11.37 %) developed the highest flexural moment with an average value of 28.72 kNm, an increase of 17 % compared to BLC beams.

The Series A and C showed incremental behaviour in the maximum compressive stress of the UHPFRC reinforcement as the beam became slenderer, unlike Series B beams where they reached a maximum and then began to decrease. The BLCHP16-C developed the maximum compressive stress in the reinforcement zone with a value of 97.88 MPa.

3.2.2. Shear behaviour

The shear stress of the sections in the central position between rollers was determined for the shorter and slenderer simulated beams (Fig. 12a). The shear stress curves in the cross-section displayed the well-known parabolic shape for timber beams and a double parabola for the composite elements with a transition zone between the materials. Due to the stress concentrations in the UHPFRC region, the shear failure occurred at the timber-concrete interface (Fig. 12b) where the timber shear strength was reached.

The evolution of shear stress along the different beams showed that for slender beams, the UHPFRC reinforcement increased the concentration of shear forces in the timber. In contrast, for short beams, there was a redistribution of shear forces toward the UHPFRC, reducing the forces in the timber members. In both cases, the stresses were much lower than the shear strength of the epoxy paste, confirming the hypothesis of no slipping between the material layers.

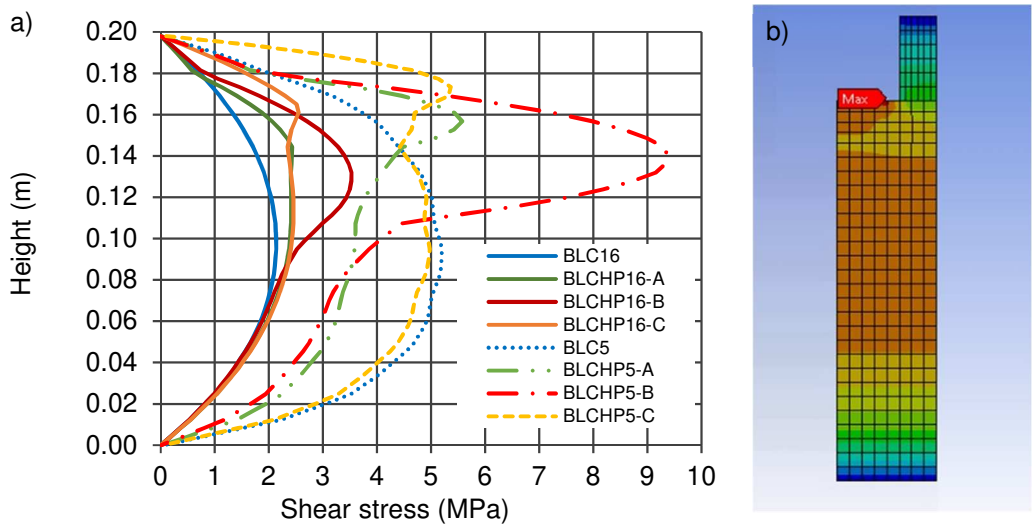

Fig. 12. Shear stress distribution in the cross-section of the beams for span = L/4

3.3. Global comparison to current materials

3.3.1. Mechanical analysis

Table 5 summarises the flexural behaviour of the beams. As expected, the steel beams have the highest load capacity and the lowest deflections among all materials. In addition, the U-G beam achieved a higher load capacity than the reinforced concrete beams, but its central deflection was almost twice as large.

Table 5. Flexural behaviour of different beams

Material	L/H	Maximum load (kN)	Deflection (mm)	Maximum flexural moment (kNm)	Normalised flexural moment μ
Glulam (BLC)	13	55.24	32.88	24.31	1.00
	16	45.81	44.09	24.28	1.00
Reinforced concrete (RC)	13	52.68	15.73	23.18	0.95
	16	43.72	22.83	23.18	0.95
HP-Glulam Series C (BLCHP)	13	65.33	30.57	28.74	1.18
	16	55.06	39.18	29.18	1.20
Steel (S)	13	118.04	9.44	51.94	2.14
	16	98.00	13.70	51.94	2.14

3.3.2. Economic and environmental results

The results of estimating unit prices for beams (Table 6) revealed that steel beams were the most expensive to produce, however, they offer higher flexural strength and stiffness. Timber beams are the most economical as they require less preparation and manufacturing processes.

Table 6. Environmental and cost performance of beams

Material	L/H	Unit price (€) (values in 2021)	Embodied energy ($kgCO_2e$)	Mass (kg)
Glulam (BLC)	13	50.45	- 27.96	20.90
	16	60.77	- 33.68	25.18
Reinforced concrete (RC)	13	109.09	15.49	132.00
	16	123.74	18.66	159.00
HP-Glulam Series C (BLCHP)	13	61.26	- 19.29	31.65
	16	73.79	- 23.24	38.12
Steel (S)	13	135.35	83.05	59.13
	16	163.04	100.04	71.23

For the U-G beam, replacing some of the timber with UHPFRC reduced the material costs; however, the processes required for the manufacturing process added an extra value to the final unit price of the element. Despite this, the BLCHP C remained the second least expensive beam.

The advantages that steel offers in mechanical terms are offset by a large amount of CO_2 required to produce it. In contrast, the beams made of wood obtained negative values, which means that they represent a benefit for the environment. This important difference is due to the production of concrete and steel, which requires large amounts of heat energy to transform the raw material. Even if the dimensions of these two materials can be reduced to achieve the flexural mechanical values of the timber or HP-Glulam beam, the embedded energy after fabrication will never be less than zero.

The most used parameter in the design of beams is the flexural moment. Therefore, the flexural moment of beams with L/H = 16 was normalised to mass, production cost, embodied energy, and deflections to evaluate the efficiency of each structural element (Fig. 13). Glulam and HP-Glulam showed the best performance for three of the four criteria (kg, €, CO_2e), with the advantage of a greater stiffness for the latter.

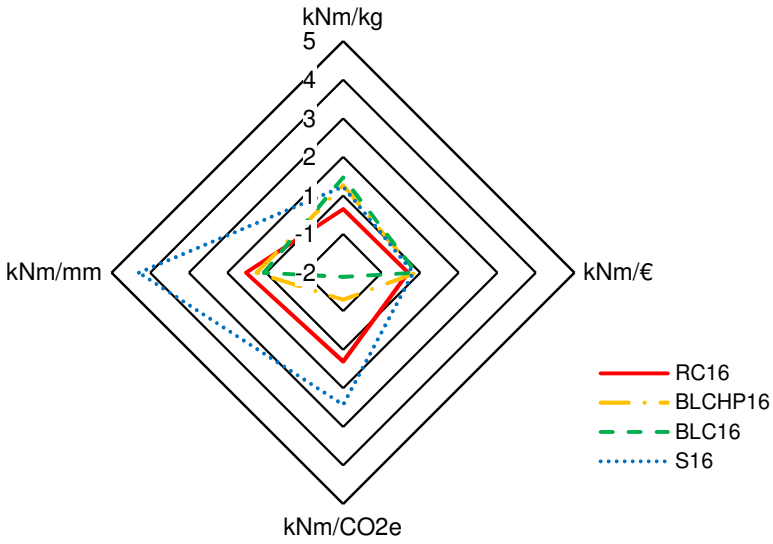

Fig. 13. Global comparison of beams

4. Conclusion

A numerical model was developed to evaluate the mechanical behaviour of the HP-Glulam, and it was completed with an economic and environmental analysis to compare its global performance with other current materials.

The Cast Iron model demonstrated a good agreement between experimental and numerical results with a difference of 8.62 % and 1.69 % for tension and flexural tests, respectively. The HP-Glulam showed linear mechanical behaviour with brittle failure in the extreme layer of the timber. Series C with one layer of UHPFRC reinforcement (ρ_{RC} = 11.37 %) at the top of the cross-section achieved the largest increase in load capacity with a difference of 20 % compared to the reference Glulam beam. Moreover, flexural failure controlled the failure of all beams from L/H = 7, and for shorter beams, the failure was controlled by the shear capacity of the timber.

Compared to reinforced concrete and steel beams, timber beams showed higher performance in terms of mass, production cost and embodied energy per kNm. In the future, slenderer L/H ratios and the cut off of UHPFRC reinforcement need to be more thoroughly investigated.

This research did not receive any specific grant from funding agencies in the public, commercial, or not-for-profit sectors

References

[1] Organisation for Economic Co-operation and Development. (2018). Global Material Resources Outlook to 2060. OECD Publishing, France.

[2] World Steel Association. (2021). Steel in buildings and infrastructure. World Steel Association. https://www.worldsteel.org/steel-by-topic/steel-markets/buildings-and-infrastructure.html

[3] World Steel Association. (2021). Climate change and the production or iron and steel. World Steel Association.

[4] Sathre R., O'Connor J. (2010). Meta-analysis of greenhouse gas displacement factors of wood product substitution. "Environmental Science and Policy", 13, 104-114.

[5] Ferrier E., Labossière P., Neale K. W. (2012). Modelling the bending behaviour of a new hybrid glulam beam reinforced with FRP and ultra-high-performance concrete. "Applied Mathematical Modelling", 36 (8), 3883-3902. https://doi.org/10.1016/j.apm.2011.11.062

[6] Titirla M.D., Ferrier E., Michel L. (2021). On the Mechanical Behaviour of Innovative Moment Connections between Composite Floor Panels and Glulam Columns. "International Journal of Architectural Heritage", 15 (2), 321-333. https://doi.org/10.1080/15583058.2020.1836529

[7] Yoo D., Yoon Y. (2016). A Review on Structural Behavior, Design, and Application of Ultra-High-Performance Fiber-Reinforced Concrete. "International Journal of Concrete Structures and Materials", 10, 125-142. https://doi.org/10.1007/s40069-016-0143-x

[8] Du H., Hu X., Han G., Shi D. (2021). Experimental and analytical investigation on flexural behaviour of glulam-concrete composite beams with interlayer. "Journal of Building Engineering". 102193. https://doi.org/10.1016/j.jobe.2021.102193

[9] Hamdolah B., Kuang J.S., Samali B. (2018). Parametric finite element analysis of RC wide beam-column connections. "Computer and Structures", 205, 28-44. https://doi.org/10.1016/j.compstruc.2018.04.004

[10] Du Y., Wei J., Liu K., Huang D., Lin Q., Yang B. (2019). Research on dynamic constitutive model of ultra-high performance fiber-reinforced concrete. "Construction and Building Materials", 234, 117386. https://doi.org/10.1016/j.conbuildmat.2019.117386

[11] Park J., Park S., Cho K., Kim S., Kwon K., Joh C. (2017). Numerical Analysis of Torsional Behavior of Ultra-High Performance Fiber Reinforced Concrete. "International Journal of Advanced Research in Science Engineering and Technology", 4(8).

[12] Jawdhari A., Fam A. (2020). Thermal-Structural Analysis and Thermal Bowing of Double Wythe UHPC Insulated Walls. "Energy and Buildings", 223, 110012. https://doi.org/10.1016/j.enbuild.2020.110012

[13] Grégoire D., Rojas-Solano L.B., Pijaudier-Cabot G. (2013). Failure and size effect for notched and unnotched concrete beams. "International Journal for Numerical and Analytical Methods in Geomechanics", 37 (10), 1434-1452. https://doi.org/10.1002/nag.2180

[14] Lee, K., Andrawes, B., Lee, J., & Kang, Y. J. (2020). Lateral Torsional Buckling of Ultra-High-Performance-Fibre-Reinforced Concrete Girders. "Magazine of Concrete Research", 72(16), 820-836. https://doi.org/10.1680/jmacr.18.00180

[15] Association Française de Génie Civil. (2013). Bétons fibrés à ultra-hautes performances – Recommandations. AFGC, France.

[16] Hassan A., Jones S., Mahmud G. (2012). Experimental test methods to determine the uniaxial tensile and compressive behaviour of ultra high performance fibre reinforced concrete (UHPFRC). "Construction and Building Materials", 37, 874-882. https://doi.org/10.1016/j.conbuildmat.2012.04.030

[17] NF P-470. (2016). Bétons. Bétons fibrés à Ultra Hautes Performances : Spécifications, performance, production et conformité. AFNOR.

[18] Blau P. (2001). The significance and use of the friction coefficient. “Tribology International”, 34 (9), 585-591. https://doi.org/10.1016/S0301-679X(01)00050-0

[19] NF P-710. (2016). Complément National à l’Eurocode 2. Calcul des structures en béton: règles spécifiques pour les Bétons Fibrés à Ultra-Hautes Performances (BFUP). AFNOR.

[20] NF EN 1995-1-1. (2005). Eurocode 5: Conception et calcul des structures en bois. Partie 1-1: généralités - règles communes et règles pour les bâtiments. AFNOR.

[21] Rammer D., Soltis L., Lebow P. (1996). Experimental shear strength of unchecked solid-sawn Douglas-Fir. US Department of Agriculture, Forest Service, Forest Products Laboratory.

[22] NF EN 1992-1-1. (2005). Eurocode 2: Calcul des structures en béton. Partie 1-1: règles générales et règles pour les bâtiments. AFNOR.

[23] NF EN 1993-1-1. (2005). Eurocode 3: Calcul des structures en acier. Partie 1-1: règles générales et règles pour les bâtiments. AFNOR.

[24] Joe C., Moustafa M., Ryan K. (2017). Cost and Ecological Feasibility of Using Ultra-High Performance Concrete in Highway Bridge Piers. Nevada Department of Transportation, United States. http://dx.doi.org/10.21838/uhpc.2016.103

[25] Centre Technique Industriel de la Construction Métallique. (2016). SAVE: Solutions Acier Valeurs Environnementales. https://www.save-construction.com/

[26] Insitut Technologique des secteurs Forêt, Cellulose, Bois-construction et Ameublement. (2019). Poutre en Douglas lamellé-collé hors aubier. FCBA, France.

[27] Centre d’études et de recherches de l’industrie du béton. (2019). Poteau en béton armé. Fiche de Déclaration Environnementale et Sanitaire. CERIB, France.

[28] Shafei B., Phares B., Sritharan S., Najimi M., Hosteng T. (2019) Laboratory and Field Evaluation of an Alternative UHPC Mix and Associated UHPC Bridge. Bridge Engineering Center: Iowa State University, United States.

[29] Stengel T., Schießl P. (2014). Life cycle assessment (LCA) of ultra high performance concrete (UHPC) structures. “Eco-efficient Construction and Building Materials”, 528-564.